Thermodynamics of SU(3) gauge theory on anisotropic lattices

doi: 10.1103/PhysRevD.64.074507

Thermodynamics of SU(3) gauge theory on anisotropic lattices

Y. Namekawa,[1] S. Aoki,[1] R. Burkhalter,[1,2] S. Ejiri,[2] M. Fukugita,[3] S. Hashimoto,[4] N. Ishizuka,[2] Y. Iwasaki,[1,2] K. Kanaya,[1] T. Kaneko,[4] Y. Kuramashi,[4] V. Lesk,[2] M. Okamoto,[2] M. Okawa,[4] Y. Taniguchi,[1] A. Ukawa,[2] and T. Yoshié[2]

(CP-PACS Collaboration)

[1]*Institute of Physics, University of Tsukuba, Tsukuba, Ibaraki 305-8571, Japan*
[2]*Center for Computational Physics, University of Tsukuba, Tsukuba, Ibaraki 305-8577, Japan*
[3]*Institute for Cosmic Ray Research, University of Tokyo, Kashiwa 277-8582, Japan*
[4]*High Energy Accelerator Research Organization (KEK), Tsukuba, Ibaraki 305-0801, Japan*

(Received 15 May 2001; published 5 September 2001)

Finite temperature SU(3) gauge theory is studied on anisotropic lattices using the standard plaquette gauge action. The equation of state is calculated on $16^3\times 8$, $20^3\times 10$, and $24^3\times 12$ lattices with the anisotropy $\xi \equiv a_s/a_t=2$, where a_s and a_t are the spatial and temporal lattice spacings. Unlike the case of the isotropic lattice on which $N_t=4$ data deviate significantly from the leading scaling behavior, the pressure and energy density on an anisotropic lattice are found to satisfy well the leading $1/N_t^2$ scaling from our coarsest lattice $N_t/\xi=4$. With three data points at $N_t/\xi=4$, 5 and 6, we perform a well controlled continuum extrapolation of the equation of state. Our results in the continuum limit agree with a previous result from isotropic lattices using the same action, but have smaller and more reliable errors.

DOI: 10.1103/PhysRevD.64.074507 PACS number(s): 11.15.Ha, 05.70.Ce, 12.38.Gc, 12.38.Mh

I. INTRODUCTION

The study of lattice QCD at finite temperatures is an important step toward clarification of the dynamics of the quark gluon plasma which is believed to have formed in the early Universe and is expected to be created in high energy heavy ion collisions [1]. In order to extract predictions for the real world from results obtained on finite lattices, we have to extrapolate lattice data to the continuum limit of vanishing lattice spacings. Because of the large computational demands for full QCD simulations, continuum extrapolations of thermodynamic quantities have so far been attempted only in SU(3) gauge theory, i.e., in the quenched approximation of QCD, where the influence of dynamical quarks is neglected. Two studies using the standard plaquette gauge action [2] and a renormalization group (RG) improved gauge action [3] have found the pressure and energy density consistent with each other in the continuum limit.

In full QCD with two flavors of dynamical quarks, thermodynamic quantities on coarse lattices have been found to show a large lattice spacing dependence [4–6]. For a reliable extrapolation to the continuum limit, data on finer lattices are required. With conventional isotropic lattices, this means an increase of the spatial lattice size to keep the physical volume close to the thermodynamic limit. Full QCD simulations on large lattices are still difficult with the current computer power. A more efficient method of calculation is desirable. Even in the quenched case, we note that continuum extrapolations of the equation of state have been made using only two lattice spacings [2,3]. In order to reliably estimate systematic errors from the extrapolations, more data points are needed. Therefore, an efficient method is also called for in quenched QCD.

Recently, anisotropic lattices have been employed to study transport coefficients and temporal correlation functions in finite temperature QCD [7–9]. In these studies, anisotropy was introduced to obtain more data points for temporal correlation functions.

In this paper, we show that anisotropic lattices also provide an efficient calculation method for thermodynamic quantities. The idea is as follows. Inspecting the free energy density of SU(3) gauge theory in the high temperature Stephan-Boltzmann limit, the leading discretization error from the temporal direction is found to be much larger than that from each of the spatial directions. Hence, choosing $\xi = a_s/a_t$ larger than one, where a_s and a_t are the spatial and temporal lattice spacings, cutoff errors in thermodynamic quantities will be efficiently reduced without much increase in the computational cost. From a study of free energy density in the high temperature limit, we find that $\xi=2$ is an optimal choice for SU(3) gauge theory. This improvement also makes it computationally easier to accumulate data for more values of temporal lattice sizes for the continuum extrapolation.

As a first test of the method, we study the equation of state (EOS) in SU(3) gauge theory. On isotropic lattices, discretization errors in the EOS for the plaquette action are quite large at the temporal lattice size $N_t=4$. The data at this value of N_t deviate significantly from the leading $1/N_t^2$ scaling behavior, $F(T)|_{N_t}=F(T)|_{\text{continuum}}+c_F/N_t^2$, where F is a thermodynamic quantity at a fixed temperature T. So far, continuum extrapolations of the EOS have been made using results at $N_t=6$ and 8. On anisotropic lattices with $\xi=2$, we find that the discretization errors in the pressure and energy density are much reduced relative to those from isotropic lattices with the same spatial lattice spacing. Furthermore, we find that the EOS at $N_t/\xi=4$, 5, and 6 follow the leading $1/N_t^2$ scaling behavior remarkably well. Therefore, a continuum extrapolation can be reliably carried out. Since the total computational cost is still lower than that for an N_t

$=8$ isotropic simulation, we can achieve higher statistics as well, resulting in smaller final errors.

In Sec. II, we study the high temperature limit of SU(3) gauge theory on anisotropic lattices to see how ξ appears in the leading discretization error for the EOS. From this study, we find that $\xi=2$ is an optimum choice for our purpose. We then perform a series of simulations on $\xi=2$ anisotropic lattices. Our lattice action and simulation parameters are described in Sec. III. Section IV is devoted to a calculation of the lattice scale through the string tension. The critical temperature is determined in Sec. V. Our main results are presented in Secs. VI and VII, where the pressure and energy density are calculated and their continuum extrapolations are carried out. A brief summary is given in Sec. VIII.

II. HIGH TEMPERATURE LIMIT

In the high temperature limit, the gauge coupling vanishes due to asymptotic freedom, and SU(3) gauge theory turns into a free bosonic gas. In the integral method [10] which we apply in this study, the pressure p is related to the free energy density f by $p=-f$ for large homogeneous systems. Therefore, in the high temperature limit, the energy density ϵ is given by $\epsilon=3p=-3f$. The value of f in the high temperature limit has been calculated in [11,12]. Normalizing ϵ by the Stephan-Boltzmann value in the continuum limit, we find

$$\frac{\epsilon}{\epsilon_{\rm SB}}=1+\frac{5+3\xi^2}{21}\left(\frac{\pi}{N_t}\right)^2+\frac{91+210\xi^2+99\xi^4}{1680}\left(\frac{\pi}{N_t}\right)^4+O\left(\left(\frac{\pi}{N_t}\right)^6\right) \tag{1}$$

for spatially large lattices. Substituting $\xi=1$ in Eq. (1), we recover the previous results for isotropic lattices [13]. When we alternatively adopt the derivative method (operator method) [11] to define the energy density, we obtain

$$\frac{\epsilon}{\epsilon_{\rm SB}}=1+\frac{5(1+\xi^2)}{21}\left(\frac{\pi}{N_t}\right)^2+\frac{13+50\xi^2+33\xi^4}{240}\left(\frac{\pi}{N_t}\right)^4+O\left(\left(\frac{\pi}{N_t}\right)^6\right). \tag{2}$$

In both formulas, the leading discretization error is proportional to $1/N_t^2$.

In the leading $1/N_t^2$ term of Eq. (1) [or Eq. (2)], the term proportional to ξ^2 represents the discretization error from finite lattice spacings a_s in the three spatial directions. We find that the temporal cutoff a_t leads to 5/8 (or 1/2) of the leading discretization error at $\xi=1$, while the spatial cutoff a_s contributes only 1/8 (or 1/6) from each of the three spatial directions.

Since a reduction of the lattice spacing in each direction separately causes an increase of the computational cost by a similar magnitude, a reduction of a_t is much more efficient than that of a_s in suppressing lattice artifacts in thermodynamic quantities. Making the anisotropy $\xi=a_s/a_t$ too large is, however, again inefficient because the spatial discretization errors remain even in the limit of $\xi=\infty$. A rough estimate for the optimum value of ξ is given by equating the discretization errors from spatial and temporal directions, $\xi=\sqrt{5}\approx 2.24$ from Eq. (1), and $\xi=\sqrt{3}\approx 1.73$ from Eq. (2). More elaborate estimations considering the balance between the computational cost as a function of the lattice size and the magnitude of discretization errors including higher orders of $1/N_t$ lead to similar values of ξ.

Based on these considerations, we adopt $\xi=2$ for simulations of SU(3) gauge theory in the present work. An even number for ξ is also attractive for the vectorization/parallelization of the simulation code, which is based on an even-odd algorithm, since we can study the case of odd N_t/ξ without modifying the program.

III. DETAILS OF SIMULATIONS

A. Action

We employ the plaquette gauge action for SU(3) gauge theory given by

$$S_G[U]=\beta\left(\frac{1}{\xi_0}Q_s+\xi_0 Q_t\right), \tag{3}$$

where ξ_0 is the bare anisotropy, $\beta=6/g_0^2$ with g_0 the bare gauge coupling constant, and

$$Q_s=\sum_{n,(ij)}(1-P_{ij}(n)),\quad Q_t=\sum_{n,i}(1-P_{i4}(n)), \tag{4}$$

with $P_{\mu\nu}(n)=\frac{1}{3}\mathrm{Re\,Tr}U_{\mu\nu}(n)$ the plaquette in the (μ,ν) plane at site n. Anisotropy is introduced by choosing $\xi_0\neq 1$.

Due to quantum fluctuations, the actual anisotropy $\xi\equiv a_s/a_t$ deviates from the bare value ξ_0. We define the renormalization factor $\eta(\beta,\xi)$ for ξ by

$$\eta(\beta,\xi)=\frac{\xi}{\xi_0(\beta,\xi)}. \tag{5}$$

The values of $\eta(\beta,\xi)$ can be determined nonperturbatively by matching Wilson loops in temporal and spatial directions on anisotropic lattices [13–16]. For our simulation, we calculate $\xi_0(\beta,\xi=2)$ using $\eta(\beta,\xi)$ obtained by Klassen for the range $1\leqslant\xi\leqslant 6$ and $5.5\leqslant\beta\leqslant\infty$ [16]:

$$\eta(\beta,\xi)=1+\left(1-\frac{1}{\xi}\right)\frac{\hat{\eta}_1(\xi)}{6}\frac{1+a_1 g_0^2}{1+a_0 g_0^2}g_0^2, \tag{6}$$

where $a_0=-0.778\,10$, $a_1=-0.550\,55$, and

$$\hat{\eta}_1(\xi)=\frac{1.002\,503\xi^3+0.391\,00\xi^2+1.471\,30\xi-0.192\,31}{\xi^3+0.262\,87\xi^2+1.590\,08\xi-0.182\,24}. \tag{7}$$

B. Simulation parameters

The main runs of our simulations are carried out on $\xi=2$ anisotropic lattices with size $N_s^3\times N_t=16^3\times 8$, $20^3\times 10$ and $24^3\times 12$. For $N_t=8$, we make additional runs on

TABLE I. Simulation parameters. Main runs are marked by asterisk (*).

Lattice	β	Bin size	No. of iterations
$12^3\times 8$	5.73–6.80	1600	40 000
$16^3\times 8$*	5.74–6.80	800	20 000
$24^3\times 8$	5.75–6.80	400	10 000
$20^3\times 10$*	5.86–6.98	2000	50 000
$24^3\times 12$*	5.95–7.20	4000	100 000
$12^3\times 24$	5.74–6.80	400	10 000
$16^3\times 32$*	5.74–6.80	200	5000
$20^3\times 40$*	5.86–6.98	500	12 500
$24^3\times 48$	5.75–5.90	100	2500
$24^3\times 48$*	5.95–7.20	1000	25 000

TABLE II. Simulation parameters for determination of critical couplings.

Lattice	β	Bin size	No. of iterations
$12^3\times 8$	5.790, 5.791	8000	80 000
$16^3\times 8$	5.790, 5.792	4000	40 000
$24^3\times 8$	5.791, 5.792	4000	40 000
$20^3\times 10$	5.903, 5.907	5000	50 000
$24^3\times 12$	6.004, 6.006	10 000	100 000

$12^3\times 8$ and $24^3\times 8$ lattices to examine finite size effects. The zero-temperature runs are made on $N_s^3\times \xi N_s$ lattices with $\xi=2$. The simulation parameters of these runs which cover the range $T/T_c\sim 0.9$–5.0 are listed in Table I. To determine precise values for the critical coupling, longer runs around the critical points are made at the parameters compiled in Table II.

For the main runs, the aspect ratio $L_sT=(N_sa_s)/(N_ta_t)$ is fixed to 4, where $L_s=N_sa_s$ is the spatial lattice size in physical units. This choice is based on a study of finite spatial volume effects presented in Sec. VI, where it is shown that, for the precision and the range of T/T_c we study, finite spatial volume effects in the EOS are sufficiently small with $L_sT\geqslant 4$.

Gauge configurations are generated by a five-hit pseudo heat bath update followed by four over-relaxation sweeps, which we call an iteration. As discussed in Sec. VI, the total number of iterations should be approximately proportional to N_t^6 to keep EOS accurate. After thermalization, we perform 20 000–100 000 iterations on finite-temperature lattices and 5000–25 000 iterations on zero-temperature lattices, as compiled in Table I. At every iteration, we measure the spatial and temporal plaquettes: $P_{\rm ss}$ and $P_{\rm st}$. Near the critical temperature, we also measure the Polyakov loop. The errors are estimated by a jack-knife method. The bin size for the jack-knife errors, listed in Table I, is determined from a study of bin size dependence as illustrated in Fig. 1. The results for the plaquettes are summarized in Tables III–V.

IV. SCALE

A. Static quark potential

We determine the physical scale of our lattices from the string tension, which is calculated from the static quark-antiquark potential at zero temperature. To calculate the static quark potential, we perform additional zero-temperature simulations listed in Table VI. The static quark potential $V(\hat{R})$ is defined through

$$W(\hat{R},\hat{T})=C(\hat{R})e^{-V(\hat{R})\hat{T}/\xi}, \tag{8}$$

where $W(\hat{R},\hat{T})$ is the Wilson loop in a spatial-temporal plane with the size $\hat{R}a_s\times\hat{T}a_t$. We measure Wilson loops at every 25 iterations after thermalization. In order to enhance the ground state signal in Eq. (8), we smear the spatial links of the Wilson loop [17,18]. Details of the smearing method are the same as in Ref. [19]. We determine the optimum smearing step $N_{\rm opt}$ which maximizes the overlap function $C(\hat{R})$

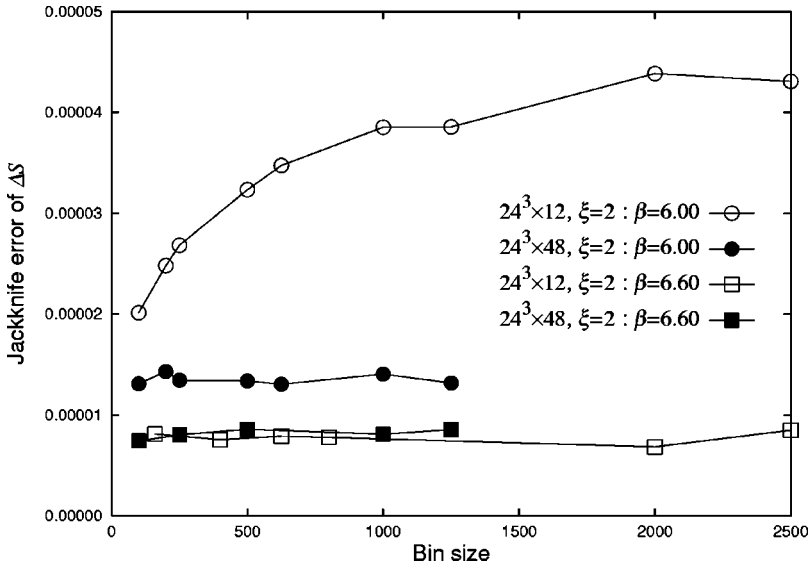

FIG. 1. Typical bin size dependence of jack-knife errors for ΔS.

TABLE III. Plaquette expectation values on $16^3\times 8$ and $16^3\times 32$ lattices with $\xi=2$.

		$16^3\times 8$		$16^3\times 32$	
β	ξ_0	P_{ss}	P_{st}	P_{ss}	P_{st}
5.740	1.662 793 18	0.448 467(31)	0.679 985(12)	0.448 490(28)	0.679 979(11)
5.750	1.664 733 08	0.450 693(24)	0.681 412(11)	0.450 641(21)	0.681 384(8)
5.760	1.666 644 10	0.452 784(33)	0.682 783(13)	0.452 731(22)	0.682 747(9)
5.770	1.668 526 93	0.454 935(29)	0.684 175(13)	0.454 758(24)	0.684 090(9)
5.780	1.670 382 23	0.457 024(53)	0.685 533(22)	0.456 720(21)	0.685 392(8)
5.788	1.671 847 08	0.459 186(116)	0.686 823(49)	0.458 272(30)	0.686 419(11)
5.790	1.672 210 65	0.459 930(109)	0.687 240(48)	0.458 678(26)	0.686 679(11)
5.792	1.672 573 16	0.460 517(104)	0.687 578(45)	0.459 056(22)	0.686 929(9)
5.800	1.674 012 80	0.462 698(75)	0.688 873(33)	0.460 586(22)	0.687 949(9)
5.805	1.674 904 22	0.463 825(34)	0.689 587(15)	0.461 565(21)	0.688 588(9)
5.810	1.675 789 29	0.464 912(40)	0.690 278(17)	0.462 446(20)	0.689 181(9)
5.820	1.677 540 71	0.466 746(21)	0.691 520(10)	0.464 241(17)	0.690 383(6)
5.830	1.679 267 62	0.468 486(24)	0.692 704(10)	0.466 022(21)	0.691 578(9)
5.840	1.680 970 58	0.470 122(18)	0.693 839(8)	0.467 707(24)	0.692 722(9)
5.880	1.687 553 24	0.476 195(15)	0.698 142(7)	0.474 205(17)	0.697 145(7)
5.900	1.690 713 95	0.478 994(18)	0.700 156(9)	0.477 282(22)	0.699 255(9)
5.950	1.698 263 59	0.485 606(15)	0.704 933(7)	0.484 390(18)	0.704 199(7)
6.000	1.705 350 29	0.491 774(15)	0.709 406(6)	0.490 955(20)	0.708 801(9)
6.100	1.718 307 38	0.503 237(14)	0.717 652(6)	0.502 986(14)	0.717 230(5)
6.200	1.729 878 92	0.513 833(11)	0.725 175(6)	0.513 839(14)	0.724 837(5)
6.300	1.740 292 71	0.523 743(10)	0.732 106(4)	0.523 915(15)	0.731 827(7)
6.400	1.749 728 20	0.533 075(11)	0.738 552(4)	0.533 401(9)	0.738 316(3)
6.500	1.758 328 76	0.541 970(13)	0.744 586(5)	0.542 362(8)	0.744 378(5)
6.600	1.766 210 35	0.550 391(8)	0.750 250(3)	0.550 854(10)	0.750 058(4)
6.700	1.773 467 85	0.558 485(9)	0.755 608(4)	0.558 959(9)	0.755 427(4)
6.800	1.780 179 64	0.566 215(12)	0.760 672(4)	0.566 716(8)	0.760 501(4)

under the condition $C(\hat{R})\leqslant 1$. Following Ref. [18], we study a local effective potential defined by

$$V_{\rm eff}(\hat{R},\hat{T})=\xi\log\left(\frac{W(\hat{R},\hat{T})}{W(\hat{R},\hat{T}+1)}\right), \tag{9}$$

which tends to $V(\hat{R})$ at sufficiently large $\hat{T}$. The reason to adopt Eq. (9) instead of the fit result from Eq. (8) is to perform a correlated error analysis directly for the potential parameters. The optimum value of $\hat{T}$, listed in Table VII, is obtained by inspecting the plateau of $V_{\rm eff}(\hat{R},\hat{T})$ at each β.

We perform a correlated fit of $V(\hat{R})=V_{\rm eff}(\hat{R},\hat{T}_{\rm opt})$ with the ansatz [20]

$$V(\hat{R})=V_0+\sigma\hat{R}-e\frac{1}{\hat{R}}+l\left(\frac{1}{\hat{R}}-\left[\frac{1}{\hat{R}}\right]\right). \tag{10}$$

Here, $[1/\hat{R}]$ is the lattice Coulomb term from one gluon exchange,

$$\left[\frac{1}{\hat{R}}\right]=4\pi\int_{-\pi}^{\pi}\frac{d^3\mathbf{k}}{(2\pi)^3}\frac{\cos(\mathbf{k}\cdot\hat{\mathbf{R}})}{4\sum_{i=1}^{3}\sin^2(k_i a_s/2)}, \tag{11}$$

which is introduced to approximately remove terms violating rotational invariance at short distances. The coefficient l is treated as a free parameter.

The fit range $[\hat{R}_{\rm min},\hat{R}_{\rm max}]$ for $\hat{R}$ is determined by consulting the stability of the fit. Our choices for $\hat{R}_{\rm min}$ are given in Table VII. We confirm that the fits and the values of the string tension are stable under a variation of $\hat{R}_{\rm min}$. The string tension is almost insensitive to a wide variation of $\hat{R}_{\rm max}$. Hence $\hat{R}_{\rm max}$ is chosen as large as possible so far as the fit is stable and the signal is not lost in the noise. With this choice for the fit range, we obtain fit curves which reproduce the data well.

Our results for the potential parameters are summarized in Table VII. The error includes the jack-knife error with bin size one (25 iterations) and the systematic error from the choice of $\hat{R}_{\rm min}$ estimated through a difference under the change of $\hat{R}_{\rm min}$ by one. We confirm that increasing the bin size to two gives consistent results on $16^3\times 32$ lattices,

TABLE IV. Plaquette expectation values on $20^3\times 10$ and $20^3\times 40$ lattices with $\xi=2$.

		$20^3\times 10$		$20^3\times 40$	
β	ξ_0	P_{ss}	P_{st}	P_{ss}	P_{st}
5.86288916	1.684 781 16	0.471 5286(90)	0.695 3072(38)	0.471 5194(98)	0.695 3039(38)
5.87	1.685 940 94	0.472 6803(97)	0.696 0907(37)	0.472 6453(79)	0.696 0771(33)
5.88583578	1.688 484 20	0.475 2043(113)	0.697 8062(52)	0.475 1072(93)	0.697 7655(41)
5.90	1.690 713 95	0.477 5533(342)	0.699 3698(144)	0.477 2612(79)	0.699 2430(33)
5.91	1.692 263 27	0.479 3349(340)	0.700 5240(144)	0.478 7235(65)	0.700 2573(30)
5.92	1.693 792 48	0.480 9915(113)	0.701 6191(50)	0.480 1832(57)	0.701 2665(26)
5.93084722	1.695 428 99	0.482 6008(89)	0.702 7227(39)	0.481 7182(78)	0.702 3359(35)
5.94	1.696 792 24	0.483 8962(61)	0.703 6250(30)	0.483 0113(60)	0.703 2314(30)
5.96	1.699 716 45	0.486 5820(62)	0.705 5225(30)	0.485 7427(62)	0.705 1382(32)
5.98	1.702 568 18	0.489 1795(54)	0.707 3650(25)	0.488 3883(83)	0.706 9900(34)
5.9961937	1.704 826 05	0.491 2217(55)	0.708 8160(30)	0.490 4832(71)	0.708 4591(30)
6.0793640	1.715 755 57	0.501 0417(44)	0.715 8270(31)	0.500 5840(62)	0.715 5576(27)
6.17716193	1.727 345 56	0.511 6532(54)	0.723 3550(25)	0.511 4357(43)	0.723 1598(22)
6.28582916	1.738 880 20	0.522 5991(56)	0.731 0157(21)	0.522 5280(53)	0.730 8687(21)
6.40118969	1.749 835 17	0.533 4631(32)	0.738 5009(19)	0.533 4926(43)	0.738 3839(17)
6.51881026	1.759 863 08	0.543 8681(48)	0.745 5581(19)	0.543 9702(40)	0.745 4657(19)
6.63417079	1.768 756 24	0.553 5144(38)	0.752 0032(19)	0.553 6476(51)	0.751 9204(23)
6.74283803	1.776 405 79	0.562 1461(45)	0.757 6970(23)	0.562 3098(36)	0.757 6251(14)
6.84063596	1.782 766 47	0.569 5876(32)	0.762 5475(17)	0.569 7626(34)	0.762 4799(11)
6.92380626	1.787 830 02	0.575 6793(33)	0.766 4882(18)	0.575 8587(31)	0.766 4206(16)
6.98915275	1.791 606 48	0.580 3248(35)	0.769 4702(14)	0.580 5094(41)	0.769 4057(18)

TABLE V. Plaquette expectation values on $24^3\times 12$ and $24^3\times 48$ lattices with $\xi=2$.

		$24^3\times 12$		$24^3\times 48$	
β	ξ_0	P_{ss}	P_{st}	P_{ss}	P_{st}
5.95	1.698 263 59	0.484 3851(27)	0.704 1916(13)	0.484 3789(45)	0.704 1883(19)
5.98	1.702 568 18	0.488 4099(39)	0.707 0003(19)	0.488 3825(35)	0.706 9880(15)
6.00	1.705 350 29	0.491 1005(118)	0.708 8537(50)	0.490 9663(38)	0.708 7977(14)
6.01	1.706 716 10	0.492 4924(104)	0.709 7962(43)	0.492 2291(37)	0.709 6838(15)
6.02	1.708 065 52	0.493 8053(64)	0.710 7011(32)	0.493 4718(30)	0.710 5575(13)
6.03	1.709 398 87	0.495 0807(40)	0.711 5881(16)	0.494 7043(36)	0.711 4232(17)
6.04	1.710 716 46	0.496 3132(30)	0.712 4510(16)	0.495 9199(32)	0.712 2791(13)
6.07	1.714 577 63	0.499 8634(27)	0.714 9595(10)	0.499 4891(31)	0.714 7889(15)
6.08	1.715 835 12	0.501 0194(19)	0.715 7747(6)	0.500 6575(31)	0.715 6082(13)
6.10	1.718 307 38	0.503 2879(22)	0.717 3807(10)	0.502 9551(29)	0.717 2208(13)
6.15	1.724 250 80	0.508 7787(26)	0.721 2576(10)	0.508 5106(19)	0.721 1154(12)
6.20	1.729 878 92	0.514 0368(26)	0.724 9549(12)	0.513 8372(20)	0.724 8368(8)
6.30	1.740 292 71	0.524 0287(21)	0.731 9188(8)	0.523 9220(23)	0.731 8284(10)
6.40	1.749 728 20	0.533 4259(25)	0.738 3798(11)	0.533 3873(23)	0.738 3125(9)
6.60	1.766 210 35	0.550 8062(15)	0.750 1014(7)	0.550 8372(22)	0.750 0563(9)
6.80	1.780 179 64	0.566 6348(15)	0.760 5281(6)	0.566 7010(21)	0.760 4924(9)
7.00	1.792 217 20	0.581 1933(20)	0.769 9251(8)	0.581 2721(12)	0.769 8933(6)
7.20	1.802 732 90	0.594 6688(17)	0.778 4726(9)	0.594 7568(18)	0.778 4435(8)

TABLE VI. Simulation parameters for static quark potential at zero temperature.

$r\beta$	Lattice	$N_{\rm opt}$	No. of configurations
5.7	$16^3\times32$	3	800
5.8	$16^3\times32$	5	800
5.9	$16^3\times32$	6	800
6.0	$16^3\times32$	8	600
	$24^3\times48$	8	100
6.1	$16^3\times32$	10	400
6.3	$16^3\times32$	16	300
	$24^3\times48$	20	100
6.5	$24^3\times48$	30	100

while, on $24^3\times48$ lattices, correlated fits with bin size two become unstable due to an insufficient number of jackknife ensembles.

B. String tension

We interpolate the string tension data using an ansatz proposed by Allton [21]:

$$a_s\sqrt{\sigma}=f(\beta)\frac{1+c_2\hat{a}(\beta)^2+c_4\hat{a}(\beta)^4}{c_0}, \tag{12}$$

where $f(\beta)$ is the two-loop scaling function of SU(3) gauge theory,

$$f(\beta)=\left(\frac{6b_0}{\beta}\right)^{-(b_1/2b_0^2)}\exp\left[-\frac{\beta}{12b_0}\right],$$

$$b_0=\frac{11}{16\pi^2},\quad b_1=\frac{102}{(16\pi^2)^2}, \tag{13}$$

and $\hat{a}(\beta)\equiv f(\beta)/f(\beta=6.0)$.

From Table VII, we find that the values for $a_s\sqrt{\sigma}$ are insensitive to the spatial lattice volume to the present precision. Using data marked by an asterisk (*) in Table VII, we obtain the best fit at

$$c_0=0.011\,71(41),\quad c_2=0.285(79),\quad c_4=0.033(30), \tag{14}$$

with $\chi^2/N_{\rm DF}=1.77$. The string tension data and the resulting fit curve are shown in Fig. 2, together with those from isotropic lattices [22].

V. CRITICAL TEMPERATURE

We define the critical gauge coupling $\beta_c(N_t,N_s)$ from the location of the peak of the susceptibility $\chi_{\rm rot}$ for a $Z(3)$-rotated Polyakov loop. The simulation parameters for the study of β_c are compiled in Table II. The β dependence of $\chi_{\rm rot}$ is calculated using the spectral density method [23]. The results for β_c are compiled in Table VIII.

To estimate the critical temperature, we have to extrapolate $\beta_c(N_t,N_s)$ to the thermodynamic limit and to the continuum limit. We perform the extrapolation to the thermodynamic limit using a finite-size scaling ansatz

$$\beta_c(N_t,N_s)=\beta_c(N_t,\infty)-h\left(\frac{N_t}{\xi N_s}\right)^3 \tag{15}$$

for first order phase transitions. From the data for β_c on anisotropic $12^3\times8$, $16^3\times8$ and $24^3\times8$ lattices with $\xi=2$, we find $h=0.031(16)$ for $N_t/\xi=4$, as shown in Fig. 3. In a previous study on isotropic lattices, h was found to be approximately independent of N_t for $N_t=4$ and 6 [24]. We extract $\beta_c(N_t,\infty)$ adopting $h=0.031(16)$ for all N_t.

The critical temperature in units of the string tension is given by

$$\frac{T_c}{\sqrt{\sigma}}=\frac{\xi}{N_t(a_s\sqrt{\sigma})(\beta_c(N_t,\infty))} \tag{16}$$

using the fit result for Eq. (12). The values of $T_c/\sqrt{\sigma}$ are summarized in Fig. 4 and Table VIII. The dominant part of the errors in $T_c/\sqrt{\sigma}$ is from the Allton fit for the string tension.

Finally we extrapolate the results to the continuum limit assuming the leading $1/N_t^2$ scaling ansatz

TABLE VII. Results for the potential parameters on $\xi=2$ anisotropic lattices with the plaquette action. The spatial lattice size L_s is computed using $\sqrt{\sigma}=440$ MeV.

β	Lattice	$a_s\sqrt{\sigma}$	L_s(fm)	$\hat{T}$	$\hat{R}_{\rm min}$	V_0	e	l	$\chi^2/N_{\rm DF}$
5.7	$16^3\times32$*	0.4794(66)	3.49	5	$\sqrt{5}$	0.677(36)	0.305(50)	0.934(122)	5.81
5.8	$16^3\times32$*	0.3804(24)	2.77	6	$\sqrt{5}$	0.720(11)	0.326(16)	0.647(49)	3.07
5.9	$16^3\times32$*	0.3190(18)	2.32	7	$\sqrt{5}$	0.688(7)	0.284(11)	0.501(43)	3.20
6.0	$16^3\times32$	0.2667(21)	1.94	8	$\sqrt{6}$	0.685(8)	0.283(14)	0.396(73)	0.93
	$24^3\times48$*	0.2611(31)	2.85	8	$\sqrt{6}$	0.699(11)	0.310(19)	0.565(82)	2.05
6.1	$16^3\times32$*	0.2224(20)	1.61	8	$2\sqrt{2}$	0.686(6)	0.297(13)	0.375(61)	1.97
6.3	$16^3\times32$	0.1656(19)	1.20	9	$\sqrt{6}$	0.653(5)	0.281(9)	0.239(67)	0.95
	$24^3\times48$*	0.1661(20)	1.81	9	$\sqrt{6}$	0.657(5)	0.294(9)	0.323(68)	1.72
6.5	$24^3\times48$*	0.1242(21)	1.35	9	$\sqrt{6}$	0.622(3)	0.279(6)	0.247(47)	1.75

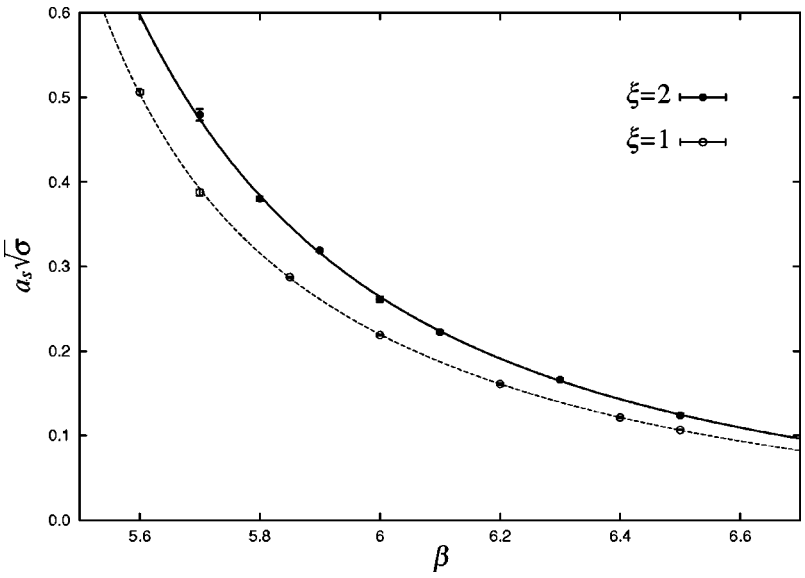

FIG. 2. String tension σ on $\xi=2$ anisotropic lattices as a function of β. Scaling fits are based on the ansatz Eq. (12).

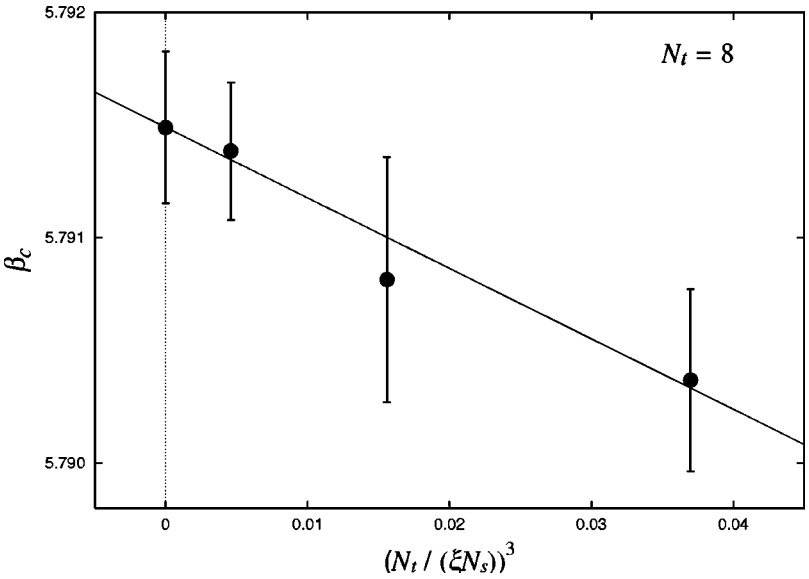

FIG. 3. Finite-size scaling of β_c for $N_t/\xi=4$ on $\xi=2$ anisotropic lattices.

TABLE VIII. Critical coupling and temperature on anisotropic $\xi=2$ lattices. Results for $T_c/\sqrt{\sigma}$ are obtained in the thermodynamic limit.

$N_s^3\times N_t$	$12^3\times 8$	$16^3\times 8$	$24^3\times 8$	$20^3\times 10$	$24^3\times 12$
$\beta_c(N_t,N_s)$	5.79037(40)	5.790 81(54)	5.79138(31)	5.904 94(92)	6.004 64(67)
$\beta_c(N_t,\infty)$		5.791 49(34)		5.905 43(116)	6.005 12(91)
$T_c/\sqrt{\sigma}$		0.6402(39)		0.6392(39)	0.6364(75)

$$F|_{N_t}=F|_{\text{continuum}}+\frac{c_F}{N_t^2}, \tag{17}$$

with $F=T_c/\sqrt{\sigma}$. The extrapolation is shown in Fig. 4. In the continuum limit, we obtain

$$\frac{T_c}{\sqrt{\sigma}}=0.635(10) \tag{18}$$

from the $\xi=2$ plaquette action.

In Fig. 4, we also plot the results obtained on isotropic lattices using the plaquette action [25] and the RG-improved action [26,3]. Our value of $T_c/\sqrt{\sigma}$ in the continuum limit is consistent with these results within the error of about 2%. A more precise comparison would require the generation and analyses of potential data in a completely parallel manner, because, as discussed in [3], numerical values of $T_c/\sqrt{\sigma}$ at a few percent level sensitively depend on the method used to determine the string tension. We leave this issue for future studies.

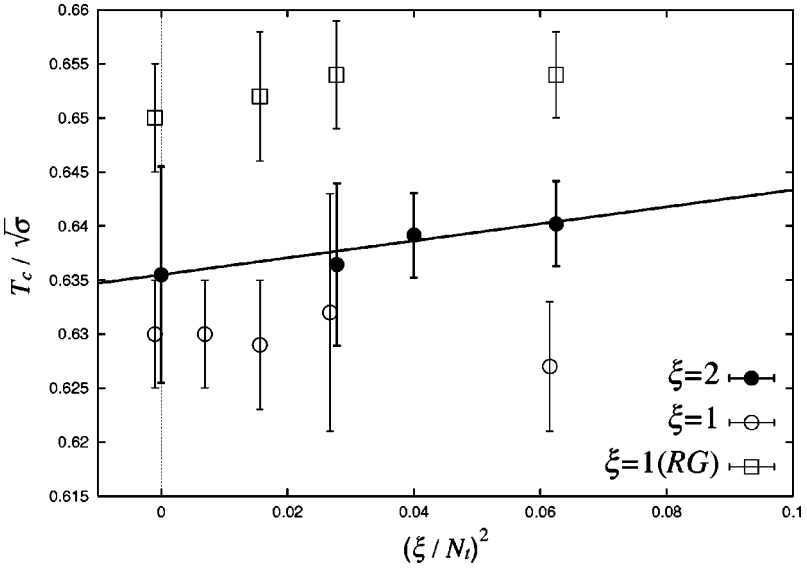

FIG. 4. Critical temperature $T_c/\sqrt{\sigma}$ on isotropic and $\xi=2$ anisotropic lattices.

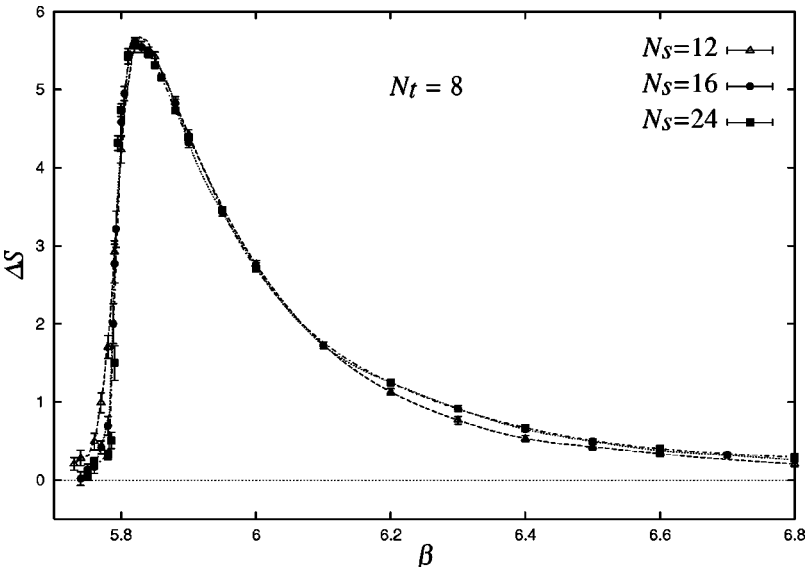

FIG. 5. Spatial lattice volume dependence in ΔS at $N_t/\xi=4$ on $N_s=12$, 16, and 24 lattices with $\xi=2$.

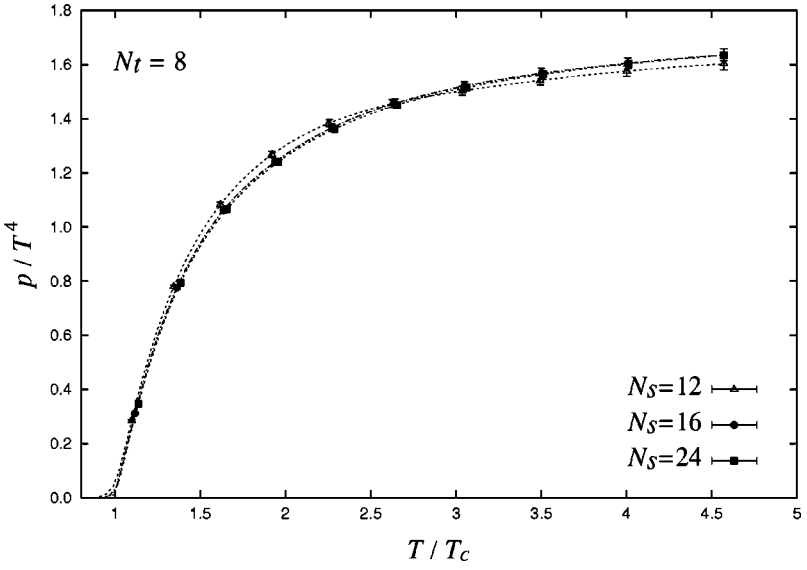

FIG. 6. Spatial volume dependence of the pressure p/T^4 on $\xi=2$ anisotropic lattices with $N_t/\xi=4$.

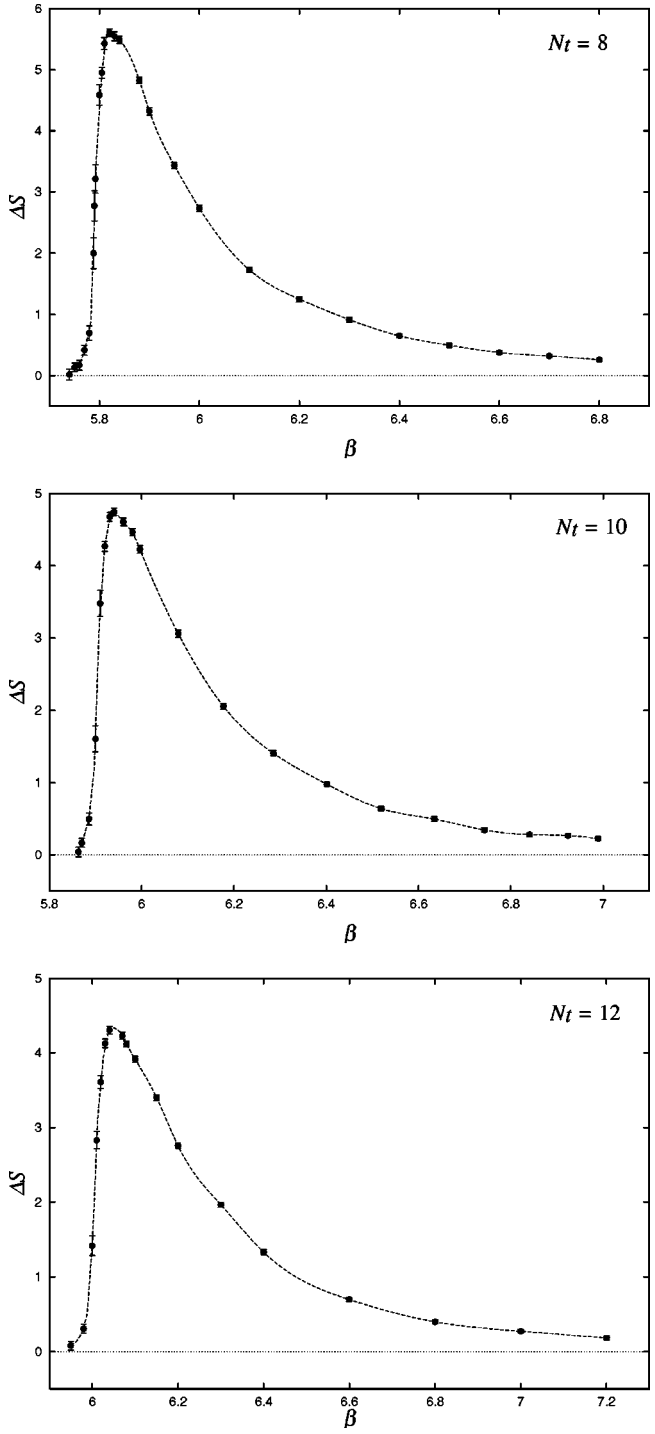

FIG. 7. ΔS on $N_t/\xi=4$, 5, and 6 lattices with $\xi=2$.

VI. PRESSURE

A. Integral method

We use the integral method to calculate the pressure [10]. This method is based on the relation $p=-f \equiv (T/V)\log Z(T,V)$ satisfied for a large homogeneous system, where $V=L_s^3$ is the spatial volume of the system in physical units and Z is the partition function. Rewriting $\log Z = \int d\beta (1/Z)(\partial Z/\partial\beta)$, the pressure is given by

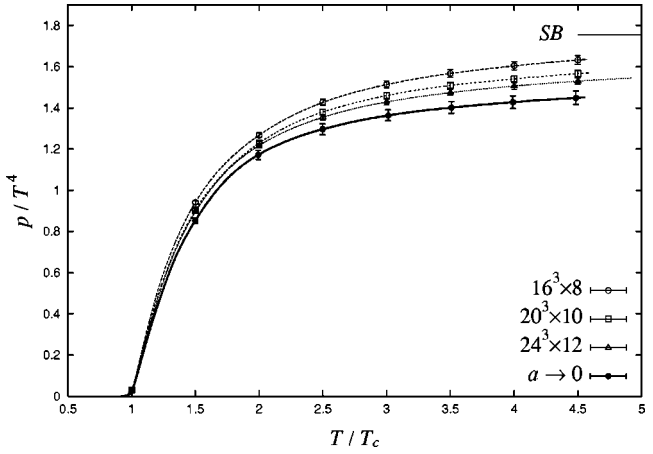

FIG. 8. Pressure p/T^4 on $\xi=2$ anisotropic lattices.

$$\left.\frac{p}{T^4}\right|_{\beta_0}^{\beta} = \int_{\beta_0}^{\beta} d\beta' \Delta S(\beta'), \tag{19}$$

with

$$\Delta S(\beta) \equiv \xi\left(\frac{N_t}{\xi}\right)^4 \frac{1}{N_s^3 N_t}\left.\frac{\partial \log Z}{\partial\beta}\right|_{\xi}. \tag{20}$$

For our anisotropic gauge action Eq. (3), the derivative of $\log Z$ is given by

$$-\frac{\partial \log Z}{\partial\beta} = \left\langle \frac{S_G}{\beta}\right\rangle + \beta\frac{\partial\xi_0(\beta,\xi)}{\partial\beta}\left(\langle Q_t\rangle - \frac{\langle Q_s\rangle}{\xi_0^2(\beta,\xi)}\right) - (T=0 \text{ contribution}). \tag{21}$$

We use symmetric $N_s^3\times\xi N_s$ lattices to calculate the $T=0$ contribution. For a sufficiently small β_0, $p(\beta_0)$ can be neglected.

In order to keep the same accuracy of ΔS for the same physical lattice volume L_s^3 in units of the temperature T, the statistics of simulations should increase in proportion to $(\xi(N_t/\xi)^4)^2/(N_s^3N_t)\propto N_t^4/\xi^3$. Here, the first factor arises from $\xi(N_t/\xi)^4$ in Eq. (20), and the second factor $1/(N_s^3N_t)$ from a suppression of fluctuations due to averaging over the lattice volume. Taking into account the autocorrelation time which is proportional to N_t^2, the number of iterations should increase as $\sim N_t^6$.

Integrating ΔS in β using a cubic spline interpolation, we obtain the pressure. For the horizontal axis, we use the temperature in units of the critical temperature

$$\frac{T}{T_c} = \frac{(a_s\sqrt{\sigma})(\beta_c)}{(a_s\sqrt{\sigma})(\beta)}. \tag{22}$$

The errors from numerical integration are estimated by a jack-knife method in the following way [3]. Since simulations at different β are statistically independent, we sum up all the contributions from β_i smaller than β corresponding to the temperature T by the naive error-propagation rule,

$\delta p(T)=\sqrt{\Sigma_i \delta p_i(T)^2}$, where $\delta_i p(T)$ at each simulation point β_i is estimated by the jackknife method.

B. Finite spatial volume effects

We first study the effects of finite spatial volume on the EOS. In Fig. 5, we show the results for ΔS at $N_t/\xi=8/2$ with the aspect ratio $L_sT=N_s\xi/N_t=3$, 4, and 6, which correspond to $N_s=12$, 16, and 24, respectively. Integrating ΔS in β, we obtain Fig. 6 for the pressure. We find that the data at $L_sT=3$ are affected by sizable finite volume effects both at $T\sim T_c$ and at high temperatures. On the other hand, for the range of T/T_c we study, the pressure does not change when the aspect ratio is increased from $L_sT=4$–6, indicating that the conventional choice $L_sT=4$ is safe with the present precision of data. Hence, we choose $L_sT=4$ for our studies of lattice spacing dependence. Results for ΔS at $L_sT=4$ with various N_t are given in Fig. 7. Integrating the data using a cubic spline interpolation, as shown in the figures, we obtain the pressure plotted in Fig. 8.

C. Continuum extrapolation

We now extrapolate the pressure to the continuum limit using the leading order ansatz of Eq. (17). Figure 9 shows the pressure at $T/T_c=1.5$, 2.5, and 3.5 as a function of $(\xi/N_t)^2$ (filled circles). For comparison, results from isotropic lattices using the plaquette action [2] (open circles) and the RG-improved action [3] (open squares) are also plotted. For the $\xi=1$ plaquette data, we adopt the results of a reanalysis made in Ref. [3] to commonly apply the scale from the Allton fit of the string tension and also the same error estimation method.

The advantage of using anisotropic lattices is apparent from Fig. 9. On the coarsest lattice $N_t/\xi=4$, finite lattice spacing errors at $\xi=2$ are much smaller than those at $\xi=1$ with the same plaquette action. The pressure at $T=2.5T_c$, for example, on the isotropic $16^3\times4$ lattice is larger than its continuum limit by about 20%, while the deviation is only 5% on the corresponding $16^3\times8$ lattice with $\xi=2$. Furthermore, with the anisotropic $\xi=2$ data, the leading $1/N_t^2$ term describes the data well even at $N_t/\xi=4$ (the rightmost point). Therefore, we can confidently perform an extrapolation to the continuum limit using three data points. In the case of the isotropic plaquette action, in contrast, the continuum extrapolation had to be made with only two data points at $N_t/\xi=6$ and 8. In the continuum limit, our results for $\xi=2$ are slightly smaller than those from the isotropic plaquette action, but the results are consistent with each other within the error of about 5% for the results from the isotropic action. It is worth observing that the $\xi=2$ results have smaller and more reliable errors of 2%–3%.

In order to quantitatively evaluate the benefit of anisotropic lattices, we compare the computational cost to achieve comparable systematic and statistical errors on isotropic and $\xi=2$ anisotropic lattices. Choosing $T=2.5T_c$ as a typical example, we find that the deviation of the pressure from the continuum limit (i.e., the magnitude of the systematic error due to finite lattice cutoffs) is comparable between the isotropic $32^3\times8$ [2] and our $\xi=2$ anisotropic $20^3\times10$ lattices, i.e., $p/T^4=1.390(26)$ on a $32^3\times8$ lattice and $p/T^4=1.381(13)$ on a $20^3\times10$ lattice, both lattices having the same spatial size $N_sa_s=1.6/T_c$. The number of configurations to achieve these statistical errors are 20 000–40 000 iterations for $\xi=1$ and 50 000 for $\xi=2$, respectively. Therefore, for the same statistical error, the relative computational cost for a $\xi=2$ lattice over that for $\xi=1$ is conservatively estimated as $((20^3\times10)\times50\,000)/((32^3\times8)\times4\times20\,000)\approx1/5$, showing a factor of 5 gain in the computational cost

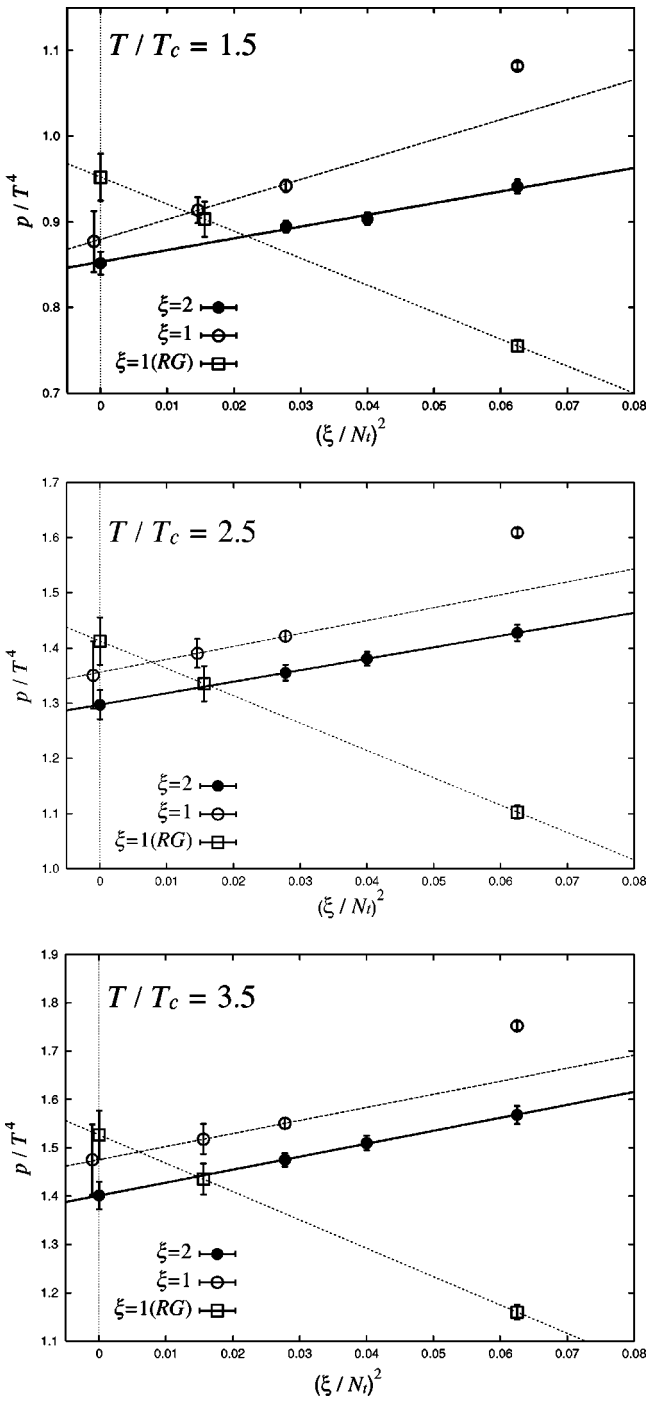

FIG. 9. Continuum extrapolation of the pressure p/T^4 at $T/T_c=1.5$, 2.5 and 3.5.

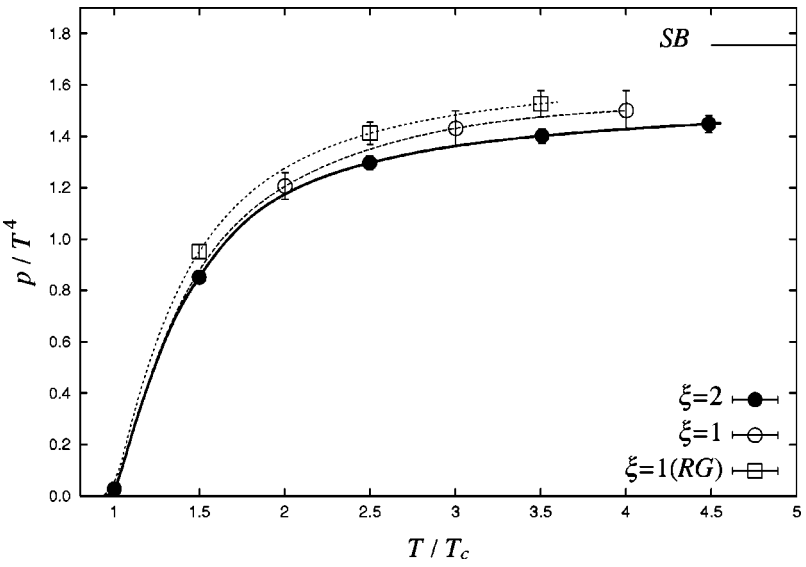

FIG. 10. Pressure p/T^4 in the continuum limit.

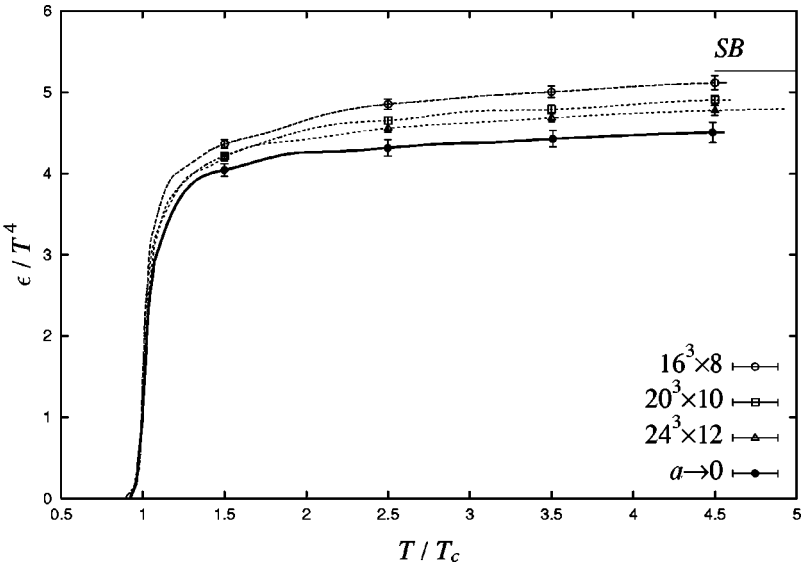

FIG. 11. ϵ/T^4 on anisotropic $16^3\times 8$, $20^3\times 10$ and $24^3\times 12$ lattices with $\xi=2$.

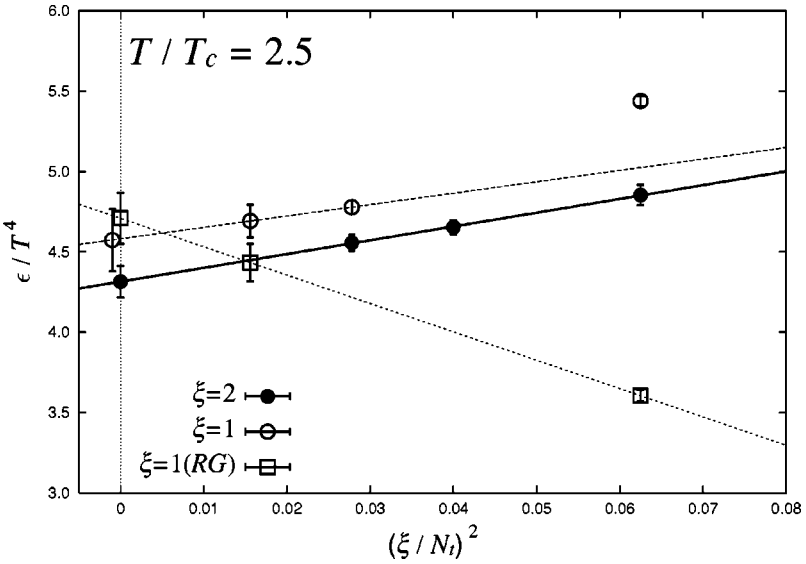

FIG. 12. Continuum extrapolation of the energy density ϵ/T^4 at $T=2.5T_c$.

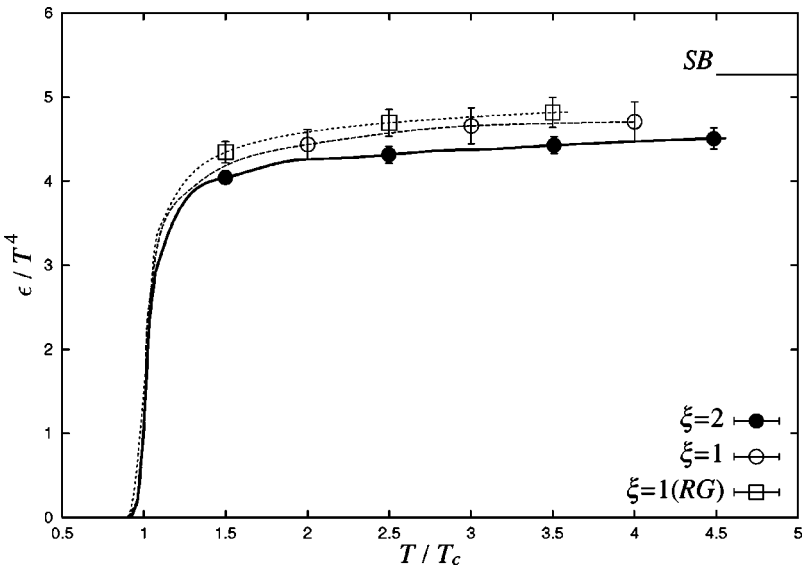

FIG. 13. Energy density ϵ/T^4 in the continuum limit.

for the anisotropic calculation in this example.

In Fig. 9 we also note that the results from the RG-improved action on isotropic lattices are higher by 7%–10% (about 2σ) than those from the present work in the continuum limit. A possible origin of this discrepancy is the use of the $N_t/\xi=4$ data of the RG-improved action, which show a large (about 20%) deviation from the continuum value. For a detailed test of consistency, we need more data points, say at $N_t/\xi=6$, from the RG-improved action.

Repeating the continuum extrapolation at other values of T/T_c, we obtain Fig. 10. Our results show a quite slow approach to the high temperature Stephan-Boltzmann limit, as reported also in previous studies on isotropic lattices [2,3].

VII. ENERGY DENSITY

We calculate the energy density ϵ by combining the results of p/T^4 with those for the interaction measure defined by

$$\frac{\epsilon-3p}{T^4}=-a_s\frac{\partial\beta}{\partial a_s}\bigg|_{\xi}\Delta S. \tag{23}$$

The QCD beta function on anisotropic lattice $\partial\beta/\partial a_s|_\xi$ is determined through the string tension σ studied in Sec. IV B,

$$a_s\frac{\partial\beta}{\partial a_s}\bigg|_{\xi}=\frac{12b_0}{6(b_1/b_0)\beta^{-1}-1}\,\frac{1+c_2\hat{a}^2+c_4\hat{a}^4}{1+3c_2\hat{a}^2+5c_4\hat{a}^4}, \tag{24}$$

where the coefficients c_i are given in Eq. (12). The error of the energy density is calculated by quadrature from the error of $3p$ and that for $\epsilon-3p$, the latter being proportional to the error of ΔS.

The results for the energy density are shown in Figs. 11 and 12. As in the case of the pressure the leading scaling behavior is well followed by our $\xi=2$ data from $N_t/\xi=4$, which allows us to extrapolate to the continuum limit reliably. The results for the energy density in the continuum limit are compared with the previous results in Fig. 13. Our $\xi=2$ plaquette action leads to an energy density which is slightly smaller than, but consistent with that from the $\xi=1$ plaquette action, but is about 7%–10% (about 2σ) smaller than that from the $\xi=1$ RG-improved action. More work is required to clarify the origin of the small discrepancy with the RG-improved action.

VIII. CONCLUSION

We have studied the continuum limit of the equation of state in SU(3) gauge theory on anisotropic lattices with the anisotropy $\xi\equiv a_s/a_t=2$, using the standard plaquette gauge action. Anisotropic lattices are shown to be more efficient in calculating thermodynamic quantities than isotropic lattices. We found that the cutoff errors in the pressure and energy density are much smaller than corresponding isotropic lattice results at small values of N_t/ξ. The computational cost for $\xi=2$ lattices is about 1/5 of that for $\xi=1$ lattices. We also found that the leading scaling behavior is well satisfied already from $N_t/\xi=4$, which enabled us to perform continuum extrapolations with three data points at $N_t/\xi=4$, 5, and 6. The equation of state in the continuum limit agrees with that obtained on the isotropic lattice using the same action, but has much smaller and better controlled errors. The benefit of anisotropic lattice demonstrated here will be indispensable for extraction of continuum predictions for the equation of state, when we include dynamical quarks.

ACKNOWLEDGMENTS

This work is supported in part by Grants-in-Aid of the Ministry of Education (Nos. 10640246, 10640248, 11640250, 11640294, 12014202, 12304011, 12640253, 12740133, 13640260). S.E. and M. Okamoto are supported by JSPS. V.L. is supported by the Research for Future Program of JSPS (Grant No. JSPS-RFTF 97P01102). Simulations were performed on the parallel computer CP-PACS at the Center for Computational Physics, University of Tsukuba.

[1] For a recent review, see S. Ejiri, Nucl. Phys. B (Proc. Suppl.) **94**, 19 (2001).
[2] G. Boyd *et al.*, Nucl. Phys. **B469**, 419 (1996).
[3] CP-PACS Collaboration, M. Okamoto *et al.*, Phys. Rev. D **60**, 094510 (1999).
[4] C. Bernard *et al.*, Phys. Rev. D **55**, 6861 (1997).
[5] J. Engels *et al.*, Phys. Lett. B **396**, 210 (1997); F. Karsch, E. Laermann, and A. Peikert, *ibid.* **478**, 447 (2000).
[6] CP-PACS Collaboration, A. Ali Khan *et al.*, Phys. Rev. D **63**, 034502 (2001); hep-lat/0103028.
[7] S. Sakai, A. Nakamura, and T. Saito, Nucl. Phys. **A638**, 535 (1998).
[8] QCD-TARO Collaboration, Ph. de Forcrand *et al.*, Phys. Rev. D **63**, 054501 (2001).
[9] T. Umeda, R. Katayama, O. Miyamura, and H. Matsufuru, Nucl. Phys. B (Proc. Suppl.) **94**, 435 (2001); hep-lat/0011085.
[10] J. Engels, J. Fingberg, F. Karsch, D. Miller, and M. Weber, Phys. Lett. B **252**, 625 (1990).
[11] J. Engels, F. Karsch, and H. Satz, Nucl. Phys. **B205**, 239 (1982).
[12] H.-Th. Elze, K. Kajantie, and J. Kapusta, Nucl. Phys. **B304**, 832 (1988).
[13] J. Engels, F. Karsch, and T. Scheideler, Nucl. Phys. **B564**, 303 (2000).
[14] G. Burgers *et al.*, Nucl. Phys. **B304**, 587 (1988).
[15] QCD-TARO Collaboration, M. Fujisaki *et al.*, Nucl. Phys. B (Proc. Suppl.) **53**, 426 (1997).
[16] T.R. Klassen, Nucl. Phys. **B533**, 557 (1998).
[17] G.S. Bali and K. Schilling, Phys. Rev. D **46**, 2636 (1992).
[18] G.S. Bali and K. Schilling, Phys. Rev. D **47**, 661 (1993).
[19] CP-PACS Collaboration, A. Ali Khan *et al.*, Phys. Rev. D **60**, 114508 (1999).
[20] C. Michael, Phys. Lett. B **283**, 103 (1992).
[21] C. Allton, hep-lat/9610016.
[22] R.G. Edwards, U.M. Heller, and T.R. Klassen, Phys. Rev. Lett. **80**, 3448 (1998).
[23] I.R. McDonald and K. Singer, Discuss. Faraday Soc. **43**, 40 (1967); A.M. Ferrenberg and R.H. Swendsen, Phys. Rev. Lett. **61**, 2635 (1988); **63**, 1195 (1989); S. Huang, K.J.M. Moriarty, E. Myers, and J. Potvin, Z. Phys. C **50**, 221 (1991).
[24] Y. Iwasaki *et al.*, Phys. Rev. D **46**, 4657 (1992).
[25] B. Beinlich, F. Karsch, E. Laermann, and A. Peikert, Eur. Phys. J. C **6**, 133 (1999).
[26] Y. Iwasaki, K. Kanaya, T. Kaneko, and T. Yoshié, Phys. Rev. D **56**, 151 (1997).